Thermosetting biocomposites of waste tea fibers and tannic acid-based epoxy

Highlights

Realizing the active role of benevolent composite materials in today's modern world, this chapter delves into various aspects of a thermosetting biocomposite by integrating modified waste tea fibers (WTFs) with tannic acid-derived epoxy (TAE). Industrial WTFs have been employed for obtaining the microfibers by treating them with alkali, followed by functionalization with maleic anhydride. The functionalization resulted in improved adhesion as well as uniform distribution of the fibers in the epoxy matrix. Two sets of biocomposite were prepared, inserting both modified and unmodified fibers in different concentrations, and they were investigated using various characterization techniques. The incorporation of modified fibers into the epoxy system resulted in enhanced tensile strength and thermal stability of the thermoset compared to unmodified ones. The biocomposites offered considerably good durability on exposure to aggressive environments such as heat (low and high temperatures), ultraviolet light, harsh chemical media, etc. and revealed biodegradable behavior upon exposure to soil.

Parts of this chapter is published in

Borah, N. and Karak, N. Green composites of bio-based epoxy and waste tea fiber as environmentally friendly structural materials. *Journal of Macromolecular Science Part A,* 60(3):217-229, 2023.

3.1. Introduction

The preceding chapter detailed the effective synthesis of a bio-based epoxy (like tannic acid-based epoxy, TAE) and its possibility as a tough, biodegradable, and benevolent thermoset. Yet, for achieving performance that can, in real life, compete with commercially available epoxy, further modification of this bio-based epoxy is imperative. Biocomposites, in this situation, stand as the top-notch solution with their advanced attributes like light weight, durability, sustainability, budget-friendly nature, etc. They have been fabricated by incorporating some additives, toughеners, or reinforcing agents into bio-based epoxy resins to ameliorate their brittleness and under-performance related issues [1, 2]. Additionally, they have been formulated to alleviate environmental hazards by practicing raw materials from natural renewable resources [3]. One such in-line reinforcement used in the production of biocomposites is natural lignocellulosic fibers, which are renewable, biodegradable, cost-effective, easily processible, and have a low density and high volume that makes them an efficient and sustainable replacement for synthetic fibers [4]. Fibers obtained from the seed, stem, and leaves of hemp, sisal, flex, jute, rice straw, coconut, etc. have been extensively utilized as reinforcing agents in the fabrication of epoxy biocomposites [5]. To add more, interesting studies presenting life cycle assessment on natural fiber-reinforced biocomposites have concluded, these materials consume about 60% less energy than synthetic alternatives, which inspires their practice for biocomposite fabrication [6].

Yet, natural tea fibers, produced in millions of tons every year in the tea factories of India and other countries as a by-product, are wasted and hence require judicious management [7]. A significant amount of research has already been dedicated to the valorization of tea waste, particularly in the area of material engineering [8, 9]. For example, cellulose nanocrystals [10], cellulose nanofibers [11], etc. were derived from the waste brewed tea leaves. A hybrid epoxy biocomposite was prepared by Prabhu et al. by employing glass, kenaf, and waste tea leaf fibers together as reinforcing agents in an epoxy matrix that showed high tensile strength (70.8 MPa) with 10% glass, 25% kenaf, and 5% tea fibers and exhibited debasement in strength with the increase of tea fiber loading [12]. This lowering of mechanical strength was attributed to the poor interaction between the matrix and the fibers, which can be improved by removing the amorphous components of the fibers or by modification. In this context, different surface modification methods including silane coupling, acrylation, $KMnO_4$ treatment, peroxide treatment, etc. were

applied to the natural fibers [13]. Maleic anhydride (MAH) is a renowned modifier and compatibilizer utilized for the grafting of natural or synthetic polymers [14]. Direct functionalization of MAH on fiber surfaces was rarely explored until Mishra et al. used it for surface modification of three different fibers by subjecting them to a 2% MAH solution for 16 h [14].

These natural fiber-reinforced biocomposites are widely explored in the fields of automobile, aerospace, and construction industries, which necessitates investigation of their durability and performance under disparate environmental conditions [15]. Alsaadi et al. studied the interlaminar fracture behavior of a glass fiber/sewage sludge ash/epoxy composite under accelerated ultraviolet (UV) radiation, which revealed a significant loss of weight and strength after 250 hours (h) of aging [16]. The durability of a coriander straw/polypropylene composite was studied in UV and hygrothermal aging conditions, where declinations were recorded in tensile, flexural, and impact strength that questioned its suitability for outdoor applications [17]. These facts demanded the design of a sustainable biocomposite that could offer superior resistance to extreme weathering conditions.

The present work, therefore, has been objectified to utilize waste tea fibers (WTFs) as reinforcing agents in a bio-based epoxy derived from tannic acid (TA) for the production of a biocomposite. Functionalization of tea fibers with MAH was primarily executed, which resulted in superior adhesion of the epoxy to the fiber surface and led to changes in their overall performance. Different aging tests were conducted to determine the weathering resistance and durability of the biocomposites against disparate environmental conditions.

3.2. Experimental

3.2.1. Materials

WTFs are generated during the conversion process of freshly harvested tea leaves into various consumable forms of tea products. Commonly, the tea leaves have to pass through five major stages before coming into consumable form: plucking, withering, rolling, oxidation and drying, and finally sorting. The WTFs are produced during the drying and sorting processes, when the tea particulates of desired sizes are extracted for packaging, with the rest fibrous parts being discarded into the environment. These tea fibers are highly

rich in polyphenols, lignin, antioxidants, and cellulose. The WTFs used in the present investigation have been collected from a local tea factory in Assam, India.

TA, epichlorohydrin, sodium hydroxide (NaOH), sodium chloride (NaCl), poly(amido amine) hardener, MAH, tetrahydrofuran (THF), and acetone were of identical specification as discussed in **Section 2.2.1** of **Chapter Two**.

3.2.2. Instrumentation

The structural analysis and property assessment of the modified and unmodified fibers and all the biocomposites were carried out by different spectroscopic, microscopic, and analytical techniques (such as FTIR, SEM, TGA, etc.) using instruments of similar specifications as described in **Section 2.2.2** of **Chapter Two**, under the same conditions. The optical microscope (Motic, UK) was used to record microscopic images. Furthermore, various mechanical properties such as tensile strength, impact strength, scratch hardness, etc. were measured using the same instruments as detailed in the previous chapter. All the tests were performed in three batches to get average results.

3.2.3. Methods

3.2.3.1. Fiber isolation and modification

The WTFs were first separated from the tea waste by repeated sieving via sieves of different pore sizes (0.5-1.5 mm). The residual fibers were then dipped in cold distilled water for 24 h to remove dirt and impurities and then dried in an oven at 50 ℃. The dried fibers were transferred to a round bottom flask with a magnetic stirrer and subsequently treated with 2% NaOH at 50 ℃ for 2 h, by maintaining a fiber-to-solution ratio of 1/25 $g.mL^{-1}$. The mixture was then vacuum filtered, washed with a 1% acetic acid solution, and washed several times with distilled water for neutralization. Finally, the fibers were washed 2-3 times with acetone and placed in an oven at 60 ℃ for drying until a constant weight was obtained and codified as MTF.

3.2.3.2. Functionalization of MTF with MAH

The mercerized tea fibers were further grafted with MAH for which 3 g of fibers were impregnated in a 3% MAH solution in acetone (1/50 $g.mL^{-1}$ fiber to solution ratio) for a period of 16 h at 65 ± 2 ℃. After completion of the process, the modified MTF (coded as MTF-g-MAH) fibers were repeatedly washed with acetone to remove the excess MAH, dried overnight at 60 ℃ and stored in a desiccator for subsequent usage.

The grafting percentage has been calculated by Soxhlet extraction of the modified fibers in acetone using **Equation 3.1**

$$\text{Grafting percentage (\%)} = [(W_2-W_1)/W_1] \times 100 \qquad \textbf{Equation 3.1}$$

where W_1 and W_2 are the amount of MTF and pure MTF-g-MAH fibers, respectively [18].

3.2.3.3. Preparation of bio-based epoxy

The bio-based resin was prepared following the same process as described in **Chapter Two** under **Section 2.2.3.1** and referred to as TAE. Similarly, the resin was cured using poly(amido amine) hardener, as explained under **Section 2.2.3.2** of the same chapter.

3.2.3.4. Fabrication of the biocomposite

The preparation of the biocomposite comprises three stages, as presented in **Figure 3.1(a)**. The first step involved wetting the fibers with the epoxy resin. An amount of 5.0 g of TAE was taken in a 100-mL beaker, and 2 mL of distilled THF was added to it to make a low-viscous resin mixture. Then 1.5 g of MTF-g-MAH (30 weight percent (wt%) of TAE) was taken in a petri dish into which the resin solution was slowly poured and mixed homogeneously with the fibers for proper wetting. The epoxy-impregnated MTF-g-MAH was kept in a vacuum desiccator at room temperature (RT) for 48 h to obtain good adhesion of the resin to the fiber surface (encoded as impMTF-g-MAH/TAE). Then, the required amount of poly(amido amine) hardener was added to the prepreg in the next step, followed by hand mixing for 10 minutes (min). The resulting content was then evenly cast inside a metal mold (inner dimensions of 10 cm × 5 cm × 0.1cm) placed above a 20 cm × 15 cm Teflon sheet and kept at RT for 24 h for the removal of free solvent.

In the third step, the content was compressed and cured by a two-step curing process. Prior to curing, the mold with prepreg was placed under vacuum for 2-3 h to remove any residual water or solvent trapped inside the prepreg. The content was then subject to compression molding in a hydraulic press under a pressure of 50-60 kN in two stages: first at 80 ± 3 ℃ for 30 min and then at 100 ℃ for 45 min. After cooling, the molded biocomposite was removed and post-cured at 120 ℃ for 30 min. **Figure 3.1(b)** represents a digital image of the final biocomposites. As depicted in **Table 3.1**, different compositions of the biocomposite were prepared following the same procedure using MTF and MTF-g-MAH as the reinforcing agents and coded as GCx or MGCx, respectively. The

x refers to the first digit of the percentage of fiber in the biocomposites with respect to the resin.

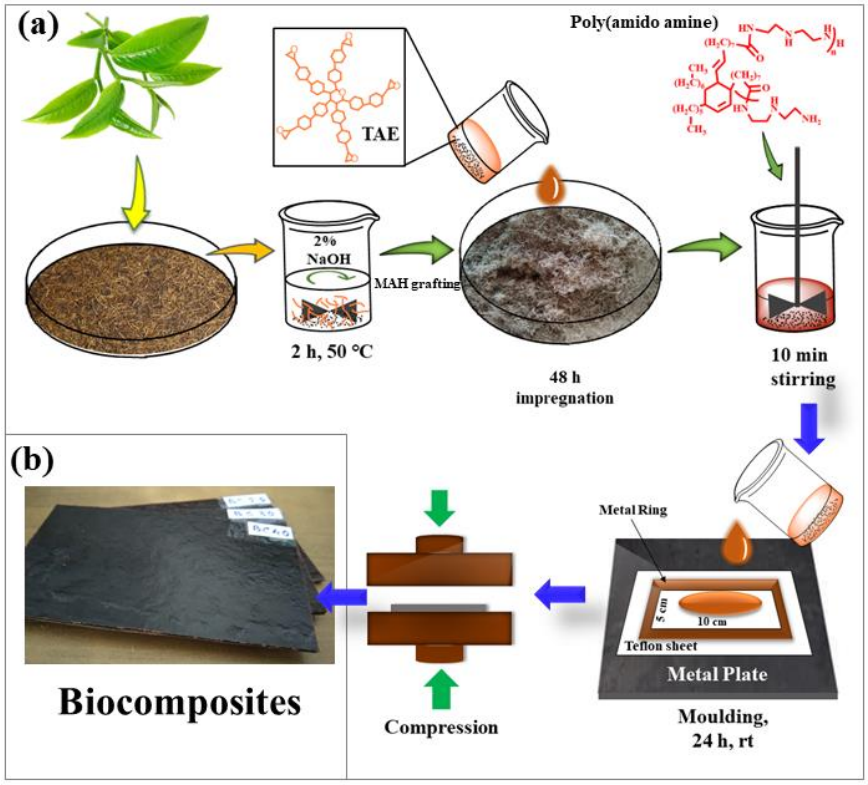

Figure 3.1: (a) Schematic representation of the steps involved in the fabrication of biocomposites and (b) digital photograph of the final biocomposites

3.2.3.5. Aging tests

To understand the suitability of the biocomposites under practical environmental conditions, samples were subject to four different artificial aging conditions: three media with different pHs, UV, two extreme temperatures, and solvent exposures, as detailed below.

(a) Chemical aging

For the aforementioned test, three rectangular specimens of each composition having dimensions 70 × 10 mm^2 were used. The specimens were separately placed in three media of variable pH, viz., acidic (pH = 4), basic (pH = 9), and neutral (pH = 7) at RT for a period of 20 days. After completion of the testing period, the specimens were taken out of the media, kept at RT for 48 h and mechanical testing was performed. Weight losses were also determined for the samples by measuring their weight before and after the tests.

Table 3.1: Compositions of the biocomposites

Sample code	TAE (g)	MTF (g)	MTF-g-MAH (g)	Poly(amido amine) (g)	Fiber to resin ratio (% of fiber w.r.t. resin)
GC2	6.0	1.2	-	2.0	1:5 (20%)
GC3	5.0	1.6	-	1.6	1:3 (30%)
GC4	4.0	1.6	-	1.5	1:2.5 (40%)
MGC2	6.0	-	1.2	2.0	1:5 (20%)
MGC3	5.0	-	1.6	1.6	1:3 (30%)
MGC4	4.0	-	1.6	1.5	1:2.5 (40%)

(b) UV aging

For the UV aging test, the specimens were placed in an accelerated UV chamber (UV Cabinet, Almicro) equilibrated with UV radiation of wavelength 256 nm and power of 8 W. The distance maintained between the samples and the UV lamp was 25 cm and the test was carried out for a duration of 150 h. After completion of the required period, the biocomposites were placed in a desiccator for 48 h and their mechanical properties were measured using an UTM.

(c) Heat aging

The biocomposites were subject to an artificial heat aging test for a period of seven days (170 h) at temperatures of 70 ± 2 ℃ and 2 ± 1 ℃ to check their durability. The tensile properties of the post-tested biocomposites were measured as earlier.

(d) Solvent aging

To study the stability of the biocomposites in organic solvents, they were immersed in EtOH and THF for a period of seven days. Afterward, their weight loss and tensile strength were measured.

The variation obtained in the mechanical strength of the biocomposites after aging is expressed in terms of elevation or retention percentages measured as follows.

$$\text{Elevation (\%)} = [(P_1 - P_0) / P_0] \times 100 \quad \textbf{Equation 3.2}$$

$$\text{Retention (\%)} = 100 - [\{(P_0 - P_1) / P_0\} \times 100] \quad \textbf{Equation 3.3}$$

where P_0 and P_1 are the initial and final strengths measured before and after aging, respectively.

3.2.3.6. Water absorption capacity

For evaluation of the water absorption capacity, the biocomposites were dried in the oven at 60 ℃ for 24 h and their weights (W_0) were recorded prior to immersing them in water at RT and at 70 ℃. The water absorbed by the biocomposites was determined in terms of weight gain by taking them out of water at a particular interval and wiping the surfaces with tissue paper, followed by measuring the weight. The biocomposites were again placed in water, and weight was measured until the saturation stage was reached. The water absorption percentages were measured as follows,

$$\text{Water absorption (\%)} = [(W_1 - W_0) / W_0] \times 100 \quad \textbf{Equation 3.4}$$

considering W_0 as the initial and W_1 as the final weight.

3.2.3.7. Soil burial test

To assess the biodegradability of the biocomposites, the soil burial test was performed, according to ASTM D570-98 standard. Previously weighted samples taken in paper cups were buried in natural soil under 10 cm depth. The test was carried out in outdoors at a temperature of 30 ± 2 ℃ and a relative humidity of 75 ± 5% for a period of 30 days. Afterward, the samples were removed, washed with distilled water, and placed in a desiccator until a constant weight was attained. The weight loss percentages were calculated according to **Equation 3.5** and the FTIR spectra of the degraded samples were recorded to monitor the changes that occurred during the test.

$$\text{Weight loss (\%)} = [(W_0 - W_1) / W_0] \times 100 \quad \textbf{Equation 3.5}$$

considering W_0 as the initial weight and W_1 as the final weight after burial.

3.3. Results and discussion

The objective of preparing the biocomposites was to add value to the tea waste produced on a huge scale every year as well as to replace the synthetic or petro-derived reinforcing agents with nature-derived ones. The advantage of these biocomposites lies in their higher bio-content compared to the TAE thermosets. The addition of 20-40% tea waste fiber as

the reinforcing agent enhanced the bio-content of the biocomposites up to 32.9-37.3% (compared to 24.7% bio-content in TAE thermoset).

The percentage of MAH present on the fiber surface, obtained after repeated washing of the fibers with acetone using Soxhlet extraction, was found to be 18.2% as calculated from **Equation 3.1**. **Figure 3.2(a)** represents the two most probable binding modes of MAH to MTF [19]. Possibly, during the modification process, the nucleophilic surface hydroxyl groups of the fiber would either open up the MAH ring, converting it to maleic acid, or bind the MAH ring to itself via hydrogen bonding [20]. Again, during impregnation of MTF-g-MAH with TAE, the carboxylic acid groups originating from MAH might be crosslinked with the epoxy rings of TAE thereby acting as an interface between TAE and the fiber in a similar way as shown in **Figure 3.2(b)**. The optical microscope images of the biocomposites clearly demonstrated the improvement in fiber dispersion, as properly distributed and aligned fibers were seen in the images of MGC4 (**Figure 3.2(d)**) compared to GC4 (**Figure 3.2(c)**). The lack of a coupling agent resulted in agglomeration between the fibers, causing an indecorous distribution throughout the matrix for GCs.

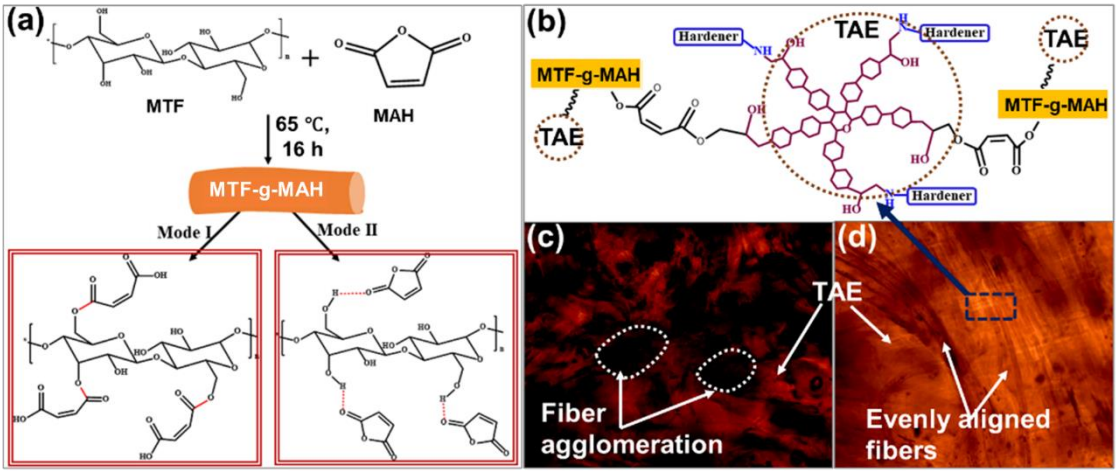

Figure 3.2: (a) Plausible mechanisms of MAH interaction with MTF, (b) crosslinking between MTF-g-MAH and TAE during impregnation, and optical microscope images of (c) GC4 and (d) MGC4 showing fiber dispersion in the matrix

3.3.1. FTIR spectral study

An FTIR spectral study was performed to obtain the structural characterization of the MTF, MTF-g-MAH, and the biocomposites. **Figure 3.3(a)** displays the FTIR spectra of MTF and MTF-g-MAH, which support the successful functionalization of MAH on the fibers. The IR bands that matched the different functionalities present in the MTF appeared as: a broad band at 3410 cm^{-1} for -OH stretching vibration of hydroxyl groups present in

cellulose as well as absorbed water; at 2915 cm^{-1} for -CH stretching; and a broad band at 1642 cm^{-1} corresponding to C=O stretching vibrations [10]. Another small peak present at 896 cm^{-1} is due to the β-glycosidic linkages between the sugar units present in the fibers [8]. The FTIR spectrum of the MTF-g-MAH exhibited characteristic peaks at 1712 cm^{-1} corresponding to the C=O group, and at 1598 cm^{-1} which corresponded to the C=C vibration of MAH moieties. Apart from these, peaks appearing at 1032 cm^{-1} (C-O stretching vibration), 863 cm^{-1} and 833 cm^{-1} (C-O-C ring stretching), and 760 cm^{-1} (ring C-H bending) supported the functionalization reaction with MAH [21]. This could also be perceived from the shifting and sharpening of the peak at 3352 cm^{-1} corresponding to -OH stretching of the surface hydroxyl groups of the fibers.

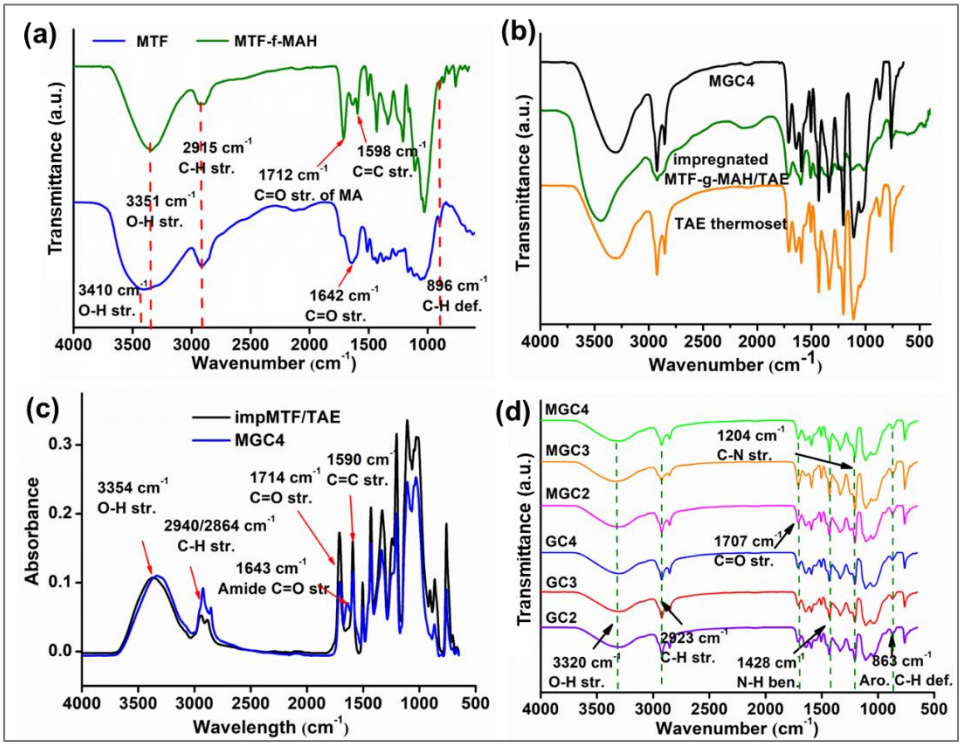

Figure 3.3: FTIR spectra of (a) MTF and MTF-g-MAH; (b) TAE, impMTF-g-MAH/TAE, and MGC4; (c) impMTF-g-MAH/TAE and MGC4; and (d) biocomposites

Figure 3.3(b) shows a comparison between the ATR-FTIR spectra of TAE thermoset, impMTF-g-MAH/TAE and MGC4. In impMTF-g-MAH/TAE, two characteristic peaks for the epoxy ring appeared in 850-910 cm^{-1} region, and a clear shift was noticed in the hydroxyl stretching peak to a higher wavenumber. To understand the bonding mechanism, a quantitative ATR-FTIR analysis was carried out for impMTF-g-MAH/TAE and MGC4 for equivalently weighted samples. From the absorbance versus wavelength plots of the samples demonstrated in **Figure 3.3(c)**, it was clear that some changes obviously occurred. In the case of impMTF-g-MAH/TAE, the absorbance

corresponding to the carbonyl peak at 1714 cm^{-1} which originated from free acids and ester groups was 0.172. While the same in MGC4 decreased to 0.102 due to the transesterification and crosslinking with epoxide rings that consumed some acidic groups. At the same time, new peaks appeared at 1641 cm^{-1} due to the formation of amide linkages from the crosslinking with the hardener. Similarly, the peak at 1590 cm^{-1} with an absorbance of 0.152 was originated from the unsaturation present in the benzene and MAH rings. The peak became less intense in MGC4 with an absorbance value of 0.118, which might have happened due to the consumption of some unsaturation via a Michaels-type reaction. Because of this interaction, strong adhesion of TAE with the MTF surface was achieved which improved their dispersion and alignment in the matrix. **Figure 3.3(d)** displays the ATR-FTIR spectra of all the biocomposites, which displayed characteristic absorption peaks, namely: 3320 cm^{-1} for -OH stretching of the hydroxyl groups of the fibers and TAE; 2923 cm^{-1} for aliphatic -CH stretching originating from cellulosic fibers and hardener; 1707 cm^{-1} for C=O stretching of MAH carbonyl and TAE ester groups; 1428 cm^{-1} for N-H bending; 1204 cm^{-1} for C-N stretching originating from the amide groups of poly(amido amine) hardener; and 863 cm^{-1} due to the aromatic C-H deformation originated from the rings present in TA of TAE, as explained in **Chapter Two**.

3.3.2. Thermal analysis

The thermal degradation profiles are presented in **Figure 3.4** and the corresponding results are tabulated in **Table 3.2**. As seen from the TGA thermograms and DTG graphs of MTF and MTF-g-MAH displayed in **Figure 3.4(a)** and **(b)**, an initial 5-10% weight loss was because of the elimination of entrapped acetone and water in the fibers. The weight loss percentage of MTF-g-MAH for this early decomposition stage was low, signifying a comparatively lower moisture content of MTF-g-MAH [22]. This might be attributed to the partial hydrophobicity induced by the functionalization of MAH on MTF, which inhabits the surface sites and thus prevents the fibers from adsorbing moisture. Nevertheless, MTF-g-MAH showed an advanced second-stage degradation profile starting from 125 ℃ to 177 ℃ with a peak degradation temperature at 155 ℃, as shown in **Figure 3.4(b)**, which can be ascribed to the breakage of MAH moieties incorporated on the fiber surface [23]. This was followed by a third degradation stage between 200 ℃ and 380 ℃ resulting from the damage of lignocellulose. Such peculiar behavior was absent in MTF, that displayed the second degradation stage for the lignocellulosic damage [24]. Moreover, the char residue obtained for the MTF-g-MAH was 1.39 times higher than the MTF,

revealing greater thermostability in the former. The evaluation of the thermal data, along with the FTIR spectral analysis, supported the success of the functionalization on MTF surface.

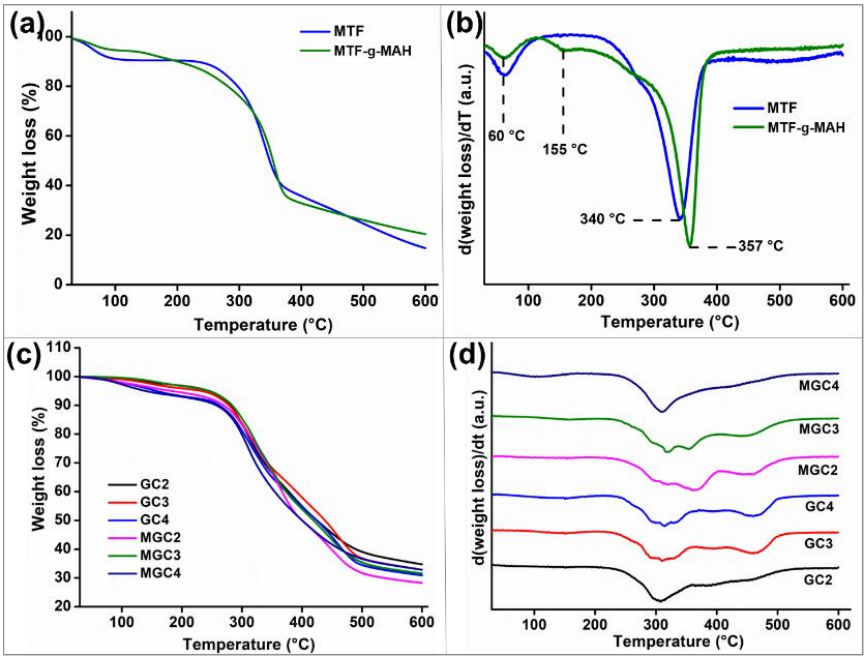

Figure 3.4: (a) TGA profiles and (b) DTG curves of MTF and MTF-g-MAH; (c) TGA and (d) DTG profiles of biocomposites

The degradation of all the GCs and MGCs commenced with an initial 2-8% weight loss within the temperature range of 50-110 ℃ which was accredited to the loss of absorbed water or solvent molecules. A clear increment (around 100 ℃) in the first degradation peak temperatures was observed in the biocomposites compared to the fibers, indicating enhanced thermostability of the materials, as shown in the TGA thermograms and DTG curves in **Figure 3.4(c)-(d)**. The better thermostability of the biocomposites MGCs compared to GCs could be attributed to the improved interfacial adhesion of the resin to the fibers after functionalization with MAH. As stated by other reported studies, modification of the fibers altered the polarity of the fibers and enhanced their miscibility over the matrix resulting in a good dispersion [25]. MGCs displayed an extended region of first-stage degradation up to a temperature of 170 ℃ owing to the decomposition of the MAH moiety present on the fiber surface. The second degradation stage between 230 ℃ and 380 ℃ was attributed to the depolymerization of lignocellulose and damage to glycosidic linkages [24]. The final degradation stage included degradation of the aromatic rings of TAE, lignin and cellulose present in the fibers, near the temperature range of 400 ℃ to 600 ℃, leading to char (weight residue) formation. The results obtained are in

alignment with the TGA profiles of some reported biocomposites, showing greater char yield and hence better thermostability of chemically treated fibers [26].

Table 3.2: Thermogravimetric parameters for the biocomposites

Parameters	GC2	GC3	GC4	MGC2	MGC3	MGC4
*T_{ON} (°C)	242	238	244	239	235	237
1st stage degradation peak temperature (°C)	306	310	313	365	320	308
2nd stage degradation peak temperature (°C)	414	463	459	460	464	-
Weight residue at 600 °C (%)	34.7	32.93	30.50	28.23	31.90	32.91

*T_{ON} refers to the onset degradation temperature

3.3.3. Mechanical properties

To appraise the effect of chemically modified fiber reinforcement on the biocomposites, the different mechanical properties of the biocomposites were determined, and the average values are listed in **Table 3.3**. The biocomposites exhibited lower tensile strength than the pristine thermoset, as shown in **Figure 3.5**. This may be due to the improper adhesion of the matrix to the fibers, especially with unmodified WTFs. The maximum tensile strengths recorded were 12.7 MPa and 16.1 MPa respectively, for GC4 and MGC4, with 40% fiber loading, whereas the pristine TAE thermoset showed a 17.2 MPa tensile strength. Similar results were obtained for a biocomposite made up of polystyrene and tea waste, where the biocomposites showed lower tensile strength than the bare polymer [27]. Other reports where WTFs were used also revealed similar results [9]. The biocomposites of tea mill waste fibers embedded in polypropylene and high-density polyethylene exhibited maximum stresses of 17.0 MPa and 22.2 MPa and strain values of 7.78% and 6.39%, respectively for 10% fiber loading [9]. For the MGCs, however, reinforcement of MTF-g-MAH imparted a bolstering effect in the biocomposites leading to improvement in the tensile strengths in comparison to the GCs of similar composition. This could be attributed to the fact that proper interfacial adhesion is required between the fibers and the resin for optimum mechanical strength, which is dependent on the surface chemisorption of the

resin on the fibers [28]. In this situation, MAH acted as an interface between the fibers and the matrix which improved the compatibility between these, otherwise incompatible components. MGC3 and MGC2 recorded a slight improvement in the tensile strength values than GC3 and GC2. Further, the MGCs showed enhancement in elongation at break values compared to the GCs owing to their improved fiber-resin bonding. Apart from the cellulosic structure present in the fibers and the aliphatic chains of poly(amido amine) hardener, the aliphatic moiety resulted from the opening of MAH rings and ester linkages might be playing a crucial role in enhancing the flexibility of the material. Similar results were also obtained in the starch-jute fiber biocomposite coated with epoxy [2].

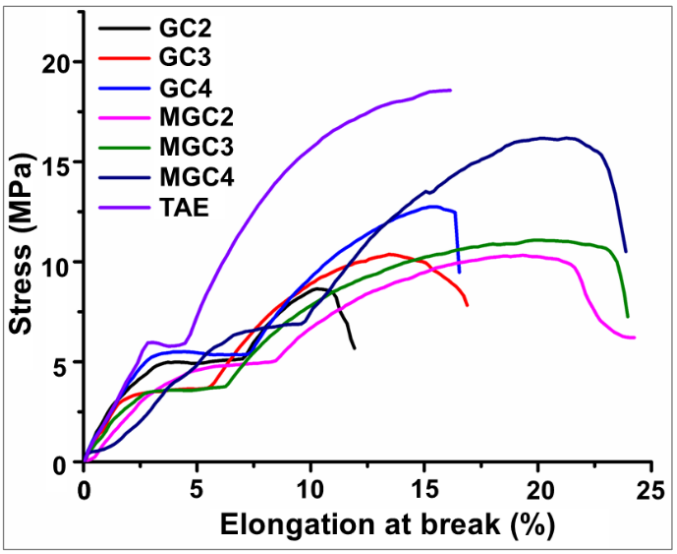

Figure 3.5: Stress-strain profiles of the biocomposites and TAE thermoset

The toughness values of the biocomposites are given in **Table 3.3** and the results displayed an increasing trend with the increase in fiber content. The MTF-g-MAH reinforcement remarkably enhanced the toughness of the biocomposites with a maximum recorded value of 231.2 J/m^3 assigned to MGC4. A similar trend was observed for the hardness (Shore A/D) values as well, which exhibited a maximum of 98 for MGC4. The impact energies of the materials were also measured by the standard falling ball method. As observed from **Table 3.3**, there was no significant differences in the impact energies of the GC2, GC3, and GC4, albeit MAH functionalization enhanced the impact energies of the MGCs. The upgraded matrix-fiber interaction via the coupling agent MAH which acted as the stress transfer agent to spread the stress from the fiber to the matrix and helped in withstanding the sudden impact experienced by the biocomposites [29]. The scratch hardness values recorded for the materials also indicated their high toughness values.

Table 3.3: Mechanical properties of the biocomposites

Sample	Tensile strength (MPa)	Elongation at break	Toughness (J/m^3)	Impact energy (kJ/m)	Scratch hardness (kg)	Hardness (Shore A/D)
GC2	8.6 ± 0.3	11.9±0.7	64.9±2.1	4.96	6	82±2
GC3	10.6 ± 0.5	16.8±2.7	112.6±5.2	4.94	6	79±3
GC4	12.7 ± 0.6	16.5±1.2	127.7±7.5	5.32	7	90±5
MGC2	10.8 ± 0.7	21.5±1.7	166.0±17.2	7.36	6	95±7
MGC3	12.3 ± 0.8	24.8±1.4	181.8±21.0	7.21	7	93±2
MGC4	16.1 ± 0.6	23.±5.2	231.2±12.3	7.53	7	98±4

3.3.4. Morphology

The SEM images of the tensile-fractured surfaces of the biocomposites were recorded for understanding the interactions of fibers with the matrix. **Figure 3.6((a)-(d))** displays the SEM images of the fractured surfaces of GC2, GC3, GC4, and MGC4, respectively. The last image explicitly revealed a considerably strong fiber-matrix bonding present between the epoxy matrix and the WTFs in MGC4. This is owing to the improved interfacial adhesion between epoxy and the MAH-treated fibers. Further, the presence of fiber bundles instead of evenly distributed fibers in the cases of GC2, GC3, and GC4 is observed in **Figure 3.6(a)-(c)**. These images also show the voids created by the pulling out of fibers. From 500× magnification of GC3 shown in **Figure 3.6(b)**, pulled-out fibers are seen, which clearly indicates the poor adhesion of fibers with the epoxy matrix. Furthermore, the distinct fiber-matrix interface observed in all three images revealed the presence of poor adhesion of the matrix to the fibers. In addition, cracks on the epoxy matrix surrounding the fiber bundles that originated from the applied load were also visible in these figures, indicating a lower crack-resisting ability of MTF in GCs. Similar kinds of fiber bundling and cracks were also observed in starch-jute/epoxy biocomposites [2]. A porous structure, matrix, and fiber breakages were observed in the pineapple, sisal fibers, and TiO_2-reinforced hybrid epoxy composite, which was due to the improper adhesion of the matrix to the fiber surface [30]. In the case of MGC4, the fiber-matrix interface clearly

suggested an adequate adhesion of the epoxy around the fibers. The imprints left by the pull-out fibers visible in the figures reflected the ability of the matrix to partially transfer the load to the fibers during the fracture under tensile load [19].

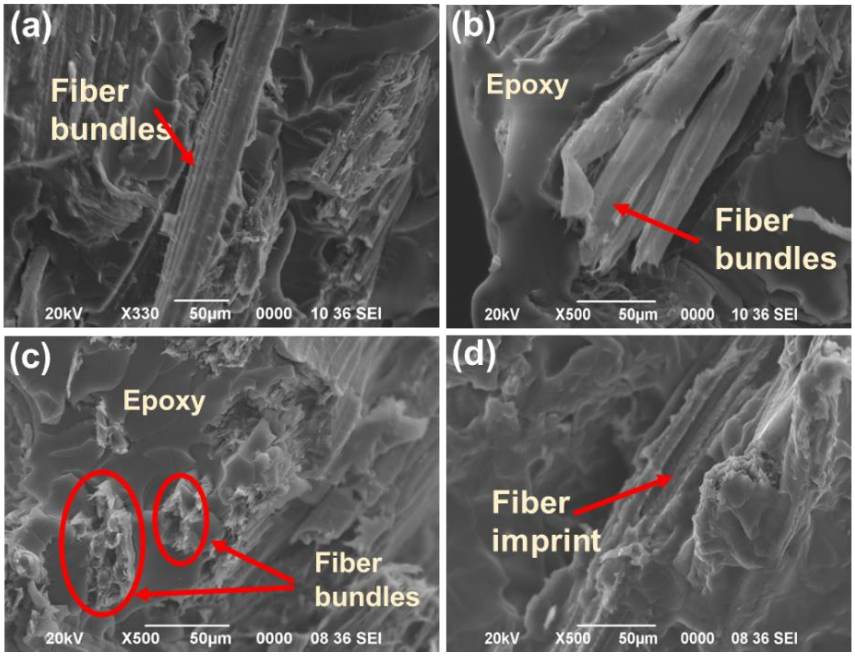

Figure 3.6: SEM images of the fractured surfaces for (a) GC2 at 330×, (b) GC3 at 500×, (c) GC4 at 500×, (d) MGC4 at 500×

3.3.5. Aging tests

For prospective applications of the designed biocomposites, evaluation of their weather resistance and durability under different environmental conditions are crucial. To inspect the same, all the biocomposites were subject to disparate aging environments. The mechanical strengths and their weight loss were determined to understand their combating ability in the post-aging process. The subsequent sub-sections described the results obtained from the different aging processes for the fabricated biocomposites.

3.3.5.1 Chemical aging

The tensile strength and weight loss values of the biocomposites after chemical aging are presented in **Figure 3.7**. The pristine thermoset suffered significant debasement in strength upon exposure to these media, as evinced by **Figure 3.7(a)**. Comparatively, the biocomposites exhibited good resistance, while marginal enhancements in the tensile strengths were observed in the acidic medium for some compositions that reflected their superiority over similar kinds of biocomposites, as reported earlier [31].

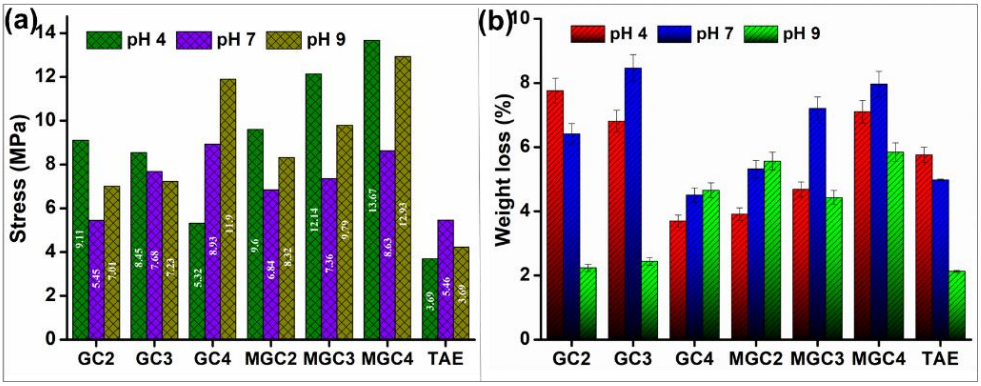

Figure 3.7: (a) Tensile strengths of the aged biocomposites and TAE thermoset at pH 4, 7, and 9; and (b) weight loss (%) profiles in the tested media

The elevation or retention percentages in tensile strength obtained after aging are presented in **Table 3.4**. The biocomposites showed elevation in tensile strengths ranging between 5.3% and 6.2% for GC2 and GC4 when exposed to the acidic medium, while others were showing declination in the same. These might have occurred due to two counteracting phenomena happening simultaneously inside the material framework. The diffusion of the solute molecules from the solution caused their inhabitation in the interstitial voids present throughout the polymer network. These residing solute molecules subsequently weakened the interfacial interaction between the matrix and fibers, decreasing the crosslinking density and hence the strength [32]. At the same time, they originated secondary crosslinking with the fibers and the epoxy network through van der Waals forces or hydrogen bonding, further rigidifying the material to offer greater mechanical strength. Moreover, the formation of new ether linkages in the acidic medium might have resulted in this improvement in tensile strength [32]. As a result, marginal changes were recorded in the biocomposites exposed to acidic media. All the compositions, however, suffered from visible debasement in their tensile strength values when exposed to neutral and alkaline media. As seen from the retentions (%) in strength from **Table 3.4**, the water and alkali molecules diffused through the fibers to the epoxy network disturbed their mutual interactions and imparted an unusual softness to the material. At pH 7, a maximum retention of 74.3% was shown by GC2, while at pH 9, GC4 showed a maximum retention of 93.5% as shown in **Table 3.4**. In parallel, the alkali and water molecules may hydrolyze the ester or ether linkages of the polymer and damage the fibers, causing notable erosion of the surface. This was reflected in the weight loss percentages of the biocomposites, as shown in **Figure 3.7(b)**. The low weight loss recorded for GCs might be explained by the presence of fiber bundles instead of evenly

Table 3.4: Elevation/retention (%) of tensile strength of the biocomposites and TAE thermoset after the aging test

Aging condition	GC2	GC3	GC4	MGC2	MGC3	MGC4	TAE
pH 4[a]	105.3	80.4	106.2	89.9	98.6	87.8	21.4
pH 7[a]	74.3	72.2	70.1	63.5	59.9	57.9	31.7
pH 9[a]	82.7	67.8	93.5	76.7	79.5	79.7	24.5
70 °C[b]	57.3	47.8	41.4	65.8	13.8	45.8	26.3
2 °C[b]	4.6	10.2	4.2	1.0	13.1	6.3	2.3
UV[b]	49.5	35.5	16.6	22.0	25.0	37.0	72.2
EtOH[a]	65.1	65.5	61.0	63.0	63.5	57.6	42.6
THF[a]	44.2	41.8	50.7	39.6	50.7	39.0	31.8

[a]Retention (%) in tensile strength, [b]Elevation (%) of tensile strength of the biocomposites.

dispersed fibers, which rendered the fibers more exposed to the solutions. Similar outcomes were reported by Saadatmanesh et al. [33], where composites made up of loose glass fiber laminates were exposed to alkaline, neutral, and acidic media (pH 12.5, 10, 7, and 2.5). Their results showed significant declination in the tensile strength values, while unidirectional and bidirectional bundled glass fiber laminates showed better performance in these solutions owing to a lower penetration rate [33].

3.3.5.2. UV and heat aging

The UV resistance of the fiber-reinforced biocomposites has been established as a crucial aspect for designing outdoor-based prospective applications. The specimens exhibited superior resistance toward UV irradiation, revealing their inordinate efficiency for exterior practices, as demonstrated in **Figure 3.8**, which shows the observed strength of the biocomposites after UV exposure. The elevation observed in the tensile strength of all the compositions ranged from 16.6 to 49.5%, as computed in **Table 3.4**. The process of UV irradiation involved a complex mechanism including chain sessions, rearrangement,

cracking of the surface, crosslinking, etc., leading to apparent stiffening of the materials. The presence of epoxy and fibers further enhanced the intricacy of the process, as both of these components performed oppositely to each other during the aging. The traces of lignocellulose present in the fibers absorbed the UV light, causing it to degrade the epoxy present around them, while the epoxy resisted the diffusion of oxygen, restricting the photodegradation of the fibers assisted by radical formation. Moreover, the antioxidants like lignin and TA present in the fibers and the resin TAE, respectively, prevented the oxidation process via a radical scavenging effect [17]. These contradicting processes presumably boosted the resistance of the biocomposites toward UV irradiation, and improvement was recorded in their tensile strengths. The earlier reported studies have also presented good resistance of epoxy biocomposites towards UV exposure and observed borderline improvements in their tensile strengths [26]. The carbon fiber epoxy composites prepared by Barbosa et al. when subject to accelerated UV aging, suffered a marginal inclination in their tensile strengths owing to the post-curing reactions occurring under UV radiation [34]. In this study, a peculiar downtrend was observed in the elongation at break values of all the biocomposites, which might be attributed to the chain scissoring followed by the rearrangement of bonds that led to improved cross-linking and thus lowered the flexibility [32].

Generally, the thermal aging of biocomposites results in marginal variations that may enhance or decrease their mechanical strengths [33, 34]. However, the prepared biocomposites showed a noticeable improvement in their tensile strengths at elevated temperatures as shown in **Figure 3.8**. The enhancement in tensile strength at 2 ℃ was negligible compared to 70 ℃. A maximum elevation of 13.1% was recorded for MGC3 at 2 ℃, while an abrupt enhancement of 65.8% at 70 ℃ was noticed for MGC2, as reflected in **Table 3.4**. These elevations could be attributed to the physicochemical changes, initiated in the biocomposites, by extreme temperature exposures. At the near-freezing temperature, the polymer chains are restricted from movement, which lowers their flexibility and increases their stiffness. This could be the reason for the observed borderline increase in tensile strength and decrease in elongation at break values. When the specimens were exposed to elevated temperatures, post-curing might have occurred in the epoxy system that increased the crosslinking density of the polymer network, offering changes in the molecular arrangements. The high crosslinking density at high temperatures resulted in embrittlement of the materials that reflected in a steep rise in their tensile strengths. The

results obtained in our study apparently symbolized the advantages of the prepared materials over other earlier reported ones for extreme temperature-based applications without compromising their performance [35].

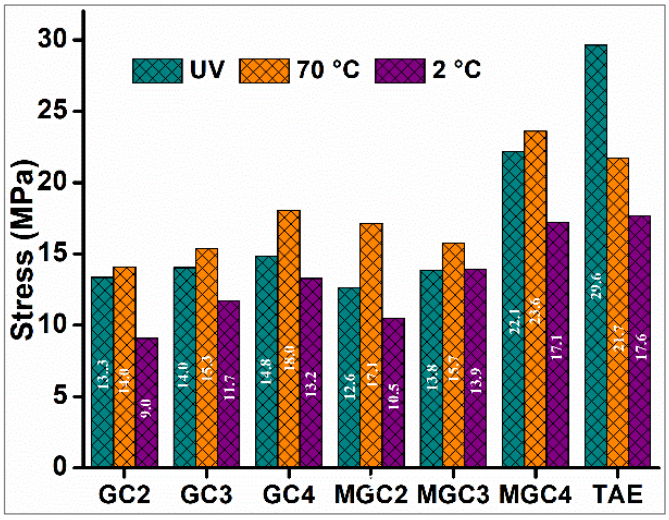

Figure 3.8: Tensile strengths of the biocomposites and TAE thermosets after UV and heat aging

Table 3.5 provides a comparison between the biocomposites and some recent reports on biocomposites in terms of changes in tensile strength after heat and UV aging. As evident from the table, the present biocomposites exhibited superior durability on exposure to extreme temperatures and UV radiation compared to others.

3.3.5.3. Solvent aging

The results obtained from solvent aging of the biocomposites are displayed in **Figure 3.9**. Due to the diffusion of solvent molecules inside the polymer network during prolonged exposure, deformations were observed in the biocomposites when immersed in THF and EtOH that resulted in a significant loss of strength, as seen from the tensile strength values in **Figure 3.9(a)**. Compared to EtOH, the effect of THF was more intense, with maximum retention of only 50.7% compared to 63.5% in EtOH as apparent from **Table 3.4**. However, the pristine thermoset displayed the maximum loss in strength in both solvents. Exposure to these solvents resulted in destructive effects on materials owing to the high solubility of the resin in THF and partial solubility in EtOH, as well as the solubility of the extractable components of the fibers in both. The solvent molecules would tend to disturb the polymer network as well as the fibers of the biocomposites to a great extent by dissolving some polymeric fractions and lignocellulosic components of the fibers. This would cause significant leaching of small fragments from the surface as well as the bulk

Table 3.5: Comparison of changes (%) in tensile strength of biocomposites under heat and UV aging with literature reports

Matrix	Reinforcing agents	Aging conditions	Change in tensile strength (%)	Ref.
Polylactic acid	Bagasse fiber	*Temp^r (-20 °C and 65 °C) for 144 h	+5.25[a]	36
Green epoxy	Basalt/Sisal fiber	Temp^r (70 °C)/UV for 340 h	-35[b]	37
Natural rubber	Nettle leaf, seeds, bark, root	Temp^r (70 °C for 14 days)/UV (72 h)	+8.7/+26.0[a]	38
Bio-epoxy	Kenaf, pineapple fiber	Temp^r (65 °C)/UV for 2 h	-19.48[b]	39
Bio-based epoxy	**WTFs**	**Temp^r (70 °C for 170 h)/UV for 150 h**	**+65.8/+49.5[a]**	**Present study**

[a]Improvement and [b]decrement in tensile strength in percentile, *Temp^r: Temperature

of the materials. This phenomenon triggered significant surface erosion and weight reductions in the biocomposites, ensuring the deterioration of their strength. The weight loss values are presented in **Figure 3.9(b)** with inset digital images of aged and unaged biocomposites, reflecting the surface erosion of samples after immersion in THF. Similar phenomena were observed in the aging study of kraft lignin-based biocomposites in water and acetone, where due to the partial solubility of lignin in acetone, significant surface erosion was noted in the latter that led to debasement in their strengths [40]. However, compared to GCs, the weight loss values were found to be lower in MGCs.

3.3.6. Water absorption

The water sorption aptitude of the biocomposites was studied by measuring the change in weight of the materials with time while being immersed in water. From the weight gain against the time of exposure plots of the materials at RT as shown in **Figure 3.10(a)**, it is evident that the biocomposites passed through a maximum sorption phase at about 15 h of contact time and then acquired an apparent saturation level after 96 h. The graphs displayed three stages of water absorption: an initial rapid absorption stage, then a relatively slower

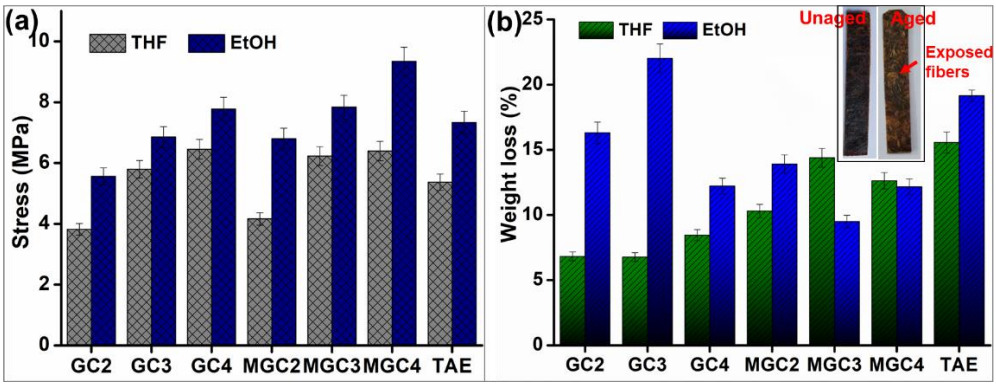

Figure 3.9: Tensile strength of the biocomposites and TAE thermoset after solvent aging in THF and EtOH, and (b) weight loss (%) with inset digital images of biocomposites showing surface erosion during solvent aging

absorption stage, followed by an asymptotic stage, which indicated a Fickian behavior to be adopted by the biocomposites. A similar three-staged water absorption behavior was observed for polylactide/sisal biocomposite in their hydrothermal aging study, which showed an increased rate of water absorption and hence physical degradation on increasing the fiber content [41]. However, the biocomposites exhibited a greater water absorption ability compared to the bare TAE thermoset, which was manifested by the presence of natural fibers in the former that would accelerate the diffusion of water through capillary action. Henceforth, the water absorption characteristics upsurged with the increasing fiber loading, ensuing a gradual rise in the weight gain of GC2<GC3<GC4. The results obtained were in consonance with other previously reported results on the water uptake behaviors of biocomposites [42]. On the contrary, the water uptake aptitudes of the MGCs were lower compared to the GCs. The MAH functionalization on the surface OH groups of the fibers would prevent the accumulation of water by occupying the fiber-matrix interface and thus lower the water absorption capacity of the biocomposites, as observed in the case of MAH-grafted polypropylene and bamboo fiber-reinforced biocomposites [19].

Furthermore, raising the immersion temperature resulted in lower water absorption by TAE thermoset and the biocomposites compared to water absorption at RT, while the saturation period was shortened to 4-5 h. At the elevated temperature, an irregularity was observed in the time versus water uptake plots of the biocomposites and the weight gain of the MGCs was found to be greater than that of the GCs. These might have happened because of the high temperature, which induced greater movement in the polymer chains, leading to softening of the materials and the formation of micro-voids over the surface. However, after attaining the maximum value, the weight gain percentages decreased

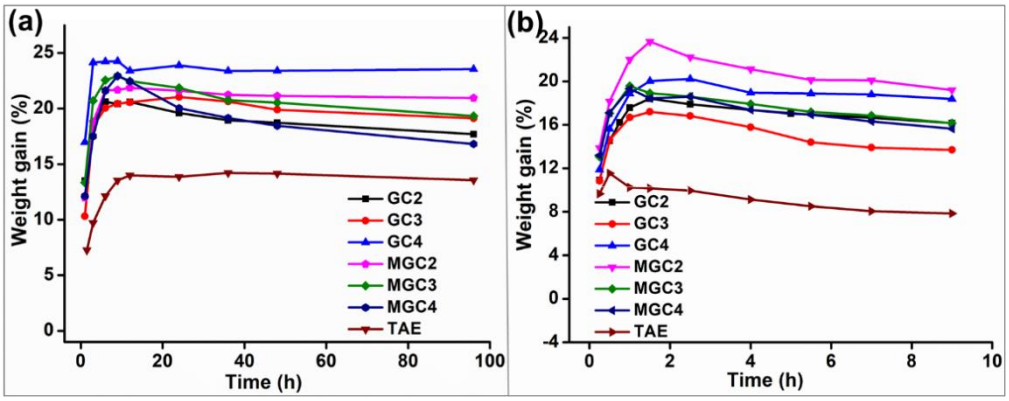

Figure 3.10: Water absorption behavior of GCs and MGCs at (a) RT and (b) 70 ℃

rapidly with increasing immersion time, as shown in **Figure 3.10(b)**, similar to some other earlier reported works [43].

3.3.7. Soil degradation

The biodegradability of the composites was investigated by evaluating their weight loss after a soil burial test conducted for 30 days. As perceived from **Figure 3.11(a)**, the weight loss increased gradually with the increase in fiber loading. The insertion of more and more fibers into the biocomposite increased the rate of moisture absorption, which further improved their biodegradable behavior. However, MTF-reinforced GCs suffered relatively higher weight loss than MTF-g-MAH-reinforced MGCs. This can be attributed to the poor fiber matrix interaction in GCs that led to greater water absorption and subsequently faster biodegradation. Additionally, the increased hydrophobicity of the fibers after MAH treatment also reduced the moisture absorption capacity of the MGCs, leading to a slower degradation rate [44]. These results are in good agreement with the previously reported studies [45]. The FTIR spectra of the degraded biocomposites were also recorded and presented in **Figure 3.11(b)**, and a slight decrease in the intensity of the different bands was visible from the figure. For obtaining a clear insight into the scenario, a comparison of the FTIR spectra of the non-degraded GC2 composite with that of the degraded GC2 composite was presented in **Figure 3.11(c)**. A significant debasement in the intensities of the peaks at 2923 cm^{-1}, 1707 cm^{-1}, and 863 cm^{-1} was noticed. These bands appeared due to the stretching vibrations of aliphatic -C-H, -C=O, and aromatic -C-H bonds, respectively, which might be due to the initial degradation of the hydrocarbon and ester linkages present in the polymeric network. Some soil microorganisms that can effortlessly degrade the hydrocarbon chains, caused partial degradation of the aliphatic -C-H linkages present in the hardener [46]. Similarly, the degradation of the ester linkages

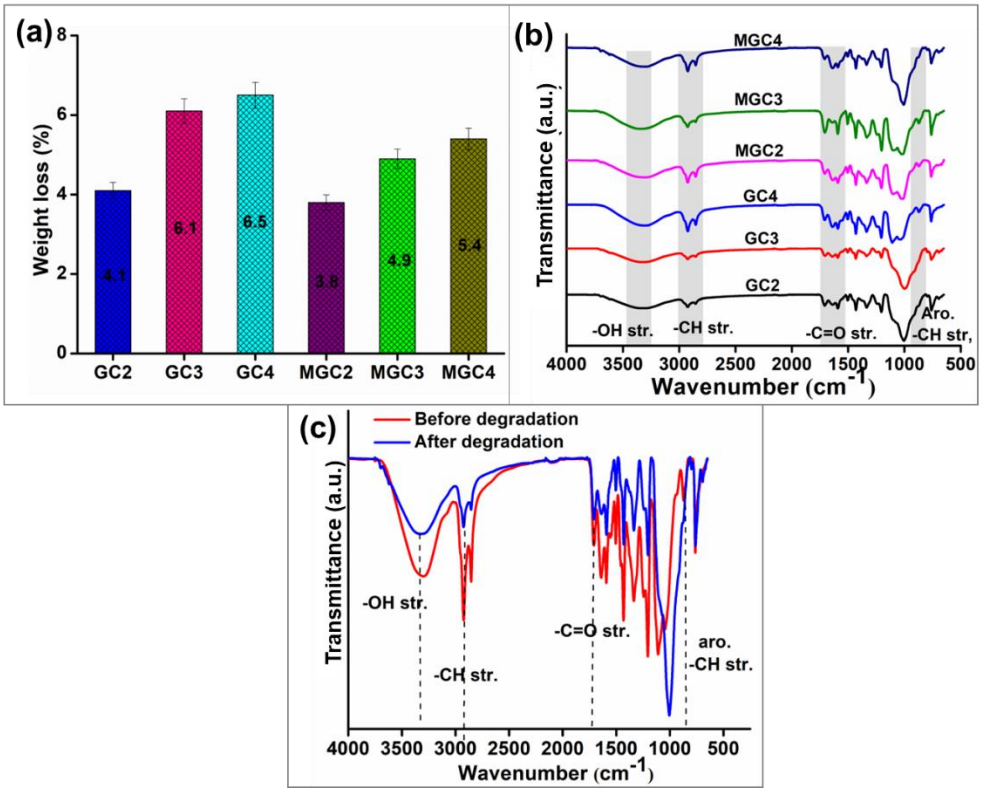

Figure 3.11: (a) Weight loss after soil burial, (b) FTIR spectra of the biocomposites after degradation, and (c) FTIR spectra of GC2 before and after soil burial

present in the TA moiety was initiated by some esterase microorganisms present in the soil [46]. However, due to the inherent antimicrobial properties of TA, some partial antimicrobial character was transferred to the biocomposites, which further slowed their rapid degradation by the soil microbes. As a result of these two counteracting forces, the rate of biodegradation of the biocomposites in the soil appeared to be slow and thus demanded a longer duration for substantial degradation to occur.

3.4. Conclusion

This study assessed the effects of MTF and MTF-g-MAH on the performance of bio-derived epoxy biocomposites as a replacement for synthetic biocomposites. Although the tensile strengths of the biocomposites were lower than those of the bare epoxy thermoset, significant improvement was recorded after modification of the fibers with MAH. The biocomposites reinforced with MAH-functionalized fibers exhibited good mechanical properties and thermal stability compared to the unmodified ones. The durability and weather resistance on exposure to different chemical and physical aging conditions demonstrated the advantages of the studied biocomposites over the pristine epoxy as well as earlier reported biocomposites. Further, a temperature-dependent water uptake behavior was noticed for the biocomposites with a short and low sorption aptitude at elevated

temperatures. However, MGCs exhibited a slower water absorption rate owing to their better interfacial adhesion compared to GCs. The overall results extended the potential applicability of these biocomposites in outdoor-based structural materials, including automobile, aerospace, and construction engineering domains.

References

[1] Ge, S., Ma, N. L., Jiang, S., Ok, Y. S., Lam, S. S., Li, C., Shi, S. Q., Nie, X., Qiu, Y., Li, D., and Wu, Q. Processed bamboo as a novel formaldehyde-free high-performance furniture biocomposite. *ACS Applied Materials & Interfaces*, 12(27):30824-30832, 2020.

[2] Verma, A., Joshi, K., Gaur, A., and Singh, V. K. Starch-jute fiber hybrid biocomposite modified with an epoxy resin coating: Fabrication and experimental characterization. *Journal of the Mechanical Behavior of Materials*, 27(5-6):20182006-20182022, 2018.

[3] Gil-Castell, O., Badia, J. D., Kittikorn, T., Strömberg, E., Martínez-Felipe, A., Ek, M., Karlsson, S., and Ribes-Greus, A. Hydrothermal ageing of polylactide/sisal biocomposites. Studies of water absorption behaviour and physico-Chemical performance. *Polymer Degradation and Stability*, 108:212-222, 2014.

[4] Ait Laaziz, S. and Hilali, E. M. Adhesion and young's modulus estimation for chemically treated argan nut shell particles reinforced poly-lactic acid polymer. *Journal of Macromolecular Science, Part B*, 59(2):77-89, 2020.

[5] Liu, W., Chen, T., Fei, M. E., Qiu, R., Yu, D., Fu, T., and Qiu, J. Properties of natural fiber-reinforced biobased thermoset biocomposites: Effects of fiber type and resin composition. *Composites Part B: Engineering*, 171:87-95, 2019.

[6] Fitzgerald, A., Proud, W., Kandemir, A., Murphy, R. J., Jesson, D. A., Trask, R. S., Hamerton, I., and Longana, M. L. A life cycle engineering perspective on biocomposites as a solution for a sustainable recovery. *Sustainability*, 13(3):1160-1185, 2021.

[7] Chowdhury, A., Sarkar, S., Chowdhury, A., Bardhan, S., Mandal, P., and Chowdhury, M. Tea waste management: A case study from West Bengal, India. *Indian Journal of Science and Technology*, 9(42):1-6, 2016.

[8] Prabhu, L., Krishnaraj, V., Sathish, S., Gokulkumar, S., Karthi, N., Rajeshkumar, L., Balaji, D., Vigneshkumar, N., Elango, K. S., Karpagam, J., and Vijayalakshmi, V. J. Experimental investigation on mechanical properties of flax/banana/industrial

waste tea leaf fiber reinforced hybrid polymer composites. *Materials Today: Proceedings*, 45:8136-8143, 2021.

[9] Dönmez Çavdar, A., Kalaycioğlu, H., and Mengeloğlu, F. Tea mill waste fibers filled thermoplastic composites: The effects of plastic type and fiber loading. *Journal of Reinforced Plastics and Composites*, 30(10):833-844, 2011.

[10] Abdul Rahman, N. H., Chieng, B. W., Ibrahim, N. A., and Abdul Rahman, N. Extraction and characterization of cellulose nanocrystals from tea leaf waste fibers. *Polymers*, 9(11):588-599, 2017.

[11] Dutta, G. K. and Karak, N. Waste brewed tea leaf derived cellulose nanofiber reinforced fully bio-based waterborne polyester nanocomposite as an environmentally benign material. *RSC Advances*, 9(36):20829-20840, 2019.

[12] Prabhu, L., Krishnaraj, V., Gokulkumar, S., Sathish, S., Sanjay, M. R., and Siengchin, S. Mechanical, chemical and sound absorption properties of glass/kenaf/waste tea leaf fiber-reinforced hybrid epoxy composites. *Journal of Industrial Textiles,* 51(10):1674-1700, 2022.

[13] Li, X., Tabil, L. G., and Panigrahi, S. Chemical treatments of natural fiber for use in natural fiber-reinforced composites: A review. *Journal of Polymers and the Environment*, 15:25-33, 2007.

[14] Mishra, S. and Naik, J. B. Effect of treatment of maleic anhydride on mechanical properties of natural fiber/polystyrene composites. *Polymer-Plastic Technology and Engineering*, 44(4):663-675, 2005.

[15] Ravikumar, P., Rajeshkumar, G., Manimegalai, P., Sumesh, K. R., Sanjay, M. R., and Siengchin, S. Delamination and surface roughness analysis of jute/polyester composites using response surface methodology: Consequence of sodium bicarbonate treatment. *Journal of Industrial Textiles*, 51:360S-377S, 2022.

[16] Alsaadi, M. and Erkliğ, A. UV accelerated aging and sewage sludge ash particle effects on mode I interlaminar fracture properties of glass fiber/epoxy composites. *Iranian Polymer Journal*, 30(8):811-820, 2021.

[17] Uitterhaegen, E., Parinet, J., Labonne, L., Mérian, T., Ballas, S., Véronèse, T., Merah, O., Talou, T., Stevens, C. V., Chabert, F., and Evon, P. Performance, durability and recycling of thermoplastic biocomposites reinforced with coriander straw. *Composites Part A: Applied Science and Manufacturing*, 113:254-263, 2018.

[18] Zhang, H. F., Zhong, H., Zhang, L. L., Chen, S. B., Zhao, Y. J., and Zhu, Y. L. Synthesis and characterization of thermosensitive graft copolymer of N-isopropylacrylamide with biodegradable carboxymethylchitosan. *Carbohydrate Polymers*, 77(4):785-790, 2009.

[19] Thwe, M. M. and Liao, K. Effects of environmental aging on the mechanical properties of bamboo–glass fiber reinforced polymer matrix hybrid composites. *Composites Part A: Applied Science and Manufacturing*, 33(1):43-52, 2002.

[20] Lv, J., Zhu, C., Qiu, H., Zhang, J., Gu, C., and Feng, J. Robust icephobic epoxy coating using maleic anhydride as a crosslinking agent. *Progress in Organic Coatings*, 142:105561-105568, 2020.

[21] Muthuraj, R., Misra, M., and Mohanty, A. K. Injection molded sustainable biocomposites from poly (butylene succinate) bioplastic and perennial grass. *ACS Sustainable Chemistry & Engineering*, 3(11):2767-2776, 2015.

[22] Tarique, J., Sapuan, S. M., and Khalina, A. Extraction and characterization of a novel natural lignocellulosic (bagasse and husk) fiber from arrowroot (*Maranta Arundinacea*). *Journal of Natural Fibers*, 19(15):9914-9930, 2022.

[23] Souza, J., Santos, A., Polese, L., Crespi, M., and Ribeiro, C. Thermal behavior of the maleic anhydride modified poly (3-hydroxybutyrate). *Journal of Thermal Analysis and Calorimetry*, 87(3):673-677, 2007.

[24] Dorez, G., Taguet, A., Ferry, L., and Lopez-Cuesta, J. M. Thermal and fire behavior of natural fibers/PBS biocomposites. *Polymer Degradation and Stability*, 98(1):87-95, 2013.

[25] El-Zayat, M. M., Abdel-Hakim, A., and Mohamed, M. A. Effect of gamma radiation on the physico mechanical properties of recycled HDPE/modified sugarcane bagasse composite. *Journal of Macromolecular Science, Part A*, 56(2):127-135, 2019.

[26] Azwa, Z. N. and Yousif, B. F. Characteristics of kenaf fibre/epoxy composites subjected to thermal degradation. *Polymer Degradation and Stability*, 98(12):2752-2759, 2013.

[27] Hussin, S. M., Alnur, N., Nik, A., Bashree, M., and Bakar, A. Potential recycling of brewed tea leaf (*Camellia Sinensis*) waste as natural reinforcement in unsaturated polyester (UPE) bio-composite. *International Journal of Advanced Science and Technology*, 28:1869-1878, 2019.

[28] Dutta, S., Karak, N., and Baruah, S. Jute-fiber-reinforced polyurethane biocomposites based on Mesua ferrea L. seed oil. *Journal of Applied Polymer Science*, 115(2):843-850, 2010.

[29] Wang, B., Hina, K., Zou, H., Cui, L., Zuo, D., and Yi, C. Mechanical, biodegradation and morphological properties of sisal fiber reinforced poly (lactic acid) biocomposites. *Journal of Macromolecular Science, Part B*, 58(2):275-289, 2019.

[30] Sumesh, K. R., Saikrishnan, G., Pandiyan, P., Prabhu, L., Gokulkumar, S., Priya, A. K., Spatenka, P., and Krishna, S. The influence of different parameters in tribological characteristics of pineapple/sisal/TiO_2 filler incorporation. *Journal of Industrial Textiles*, 51:8626S-8644S, 2022.

[31] Wang, J. U. N., Gangarao, H. O. T. A., Liang, R., and Liu, W. Durability and prediction models of fiber-reinforced polymer composites under various environmental conditions: A critical review. *Journal of Reinforced Plastics and Composites*, 35(3):179-211, 2016.

[32] Dutta, G. K. and Karak, N. One-pot synthesis of bio-based waterborne polyester as UV-resistant biodegradable sustainable material with controlled release attributes. *ACS Omega*, 3(12):16812-16822, 2018.

[33] Karakuzu, R., Kanlioglu, H., and Deniz, M. E. Environmental effects on mechanical properties of glass-epoxy composites. *Materials Testing*, 56(5):355-361, 2014.

[34] Barbosa, A. P. C., Fulco, A. P. P., Guerra, E. S., Arakaki, F. K., Tosatto, M., Costa, M. C. B., and Melo, J. D. D. Accelerated aging effects on carbon fiber/epoxy composites. *Composites Part B: Engineering*, 110:298-306, 2017.

[35] Yang, Y., Xian, G., Li, H., and Sui, L. Thermal aging of an anhydride-cured epoxy resin. *Polymer Degradation and Stability*, 118:111-119, 2015.

[36] Lila, M. K., Shukla, K., Komal, U. K., and Singh, I. Accelerated thermal ageing behaviour of bagasse fibers reinforced poly(Lactic Acid) based biocomposites. *Composites Part B: Engineering*, 156:121-127, 2019.

[37] Zuccarello, B., Bongiorno, F., and Militello, C. Basalt fiber hybridization effects on high-performance sisal-reinforced biocomposites. *Polymers*, 14(7):1457-1473, 2022.

[38] Masłowski, M., Aleksieiev, A., Miedzianowska, J., and Strzelec, K. Common nettle (*Urtica dioica* L.) as an active filler of natural rubber biocomposites. *Materials*, 14(7):1616-1646, 2021.

[39] Kumar, S., Saha, A., and Bhowmik, S. Accelerated weathering effects on mechanical, thermal and viscoelastic properties of kenaf/pineapple biocomposite laminates for load bearing structural applications. *Journal of Applied Polymer Science*, 139(2):51465-51481, 2022.

[40] Klapiszewski, Ł., Podkościelna, B., Goliszek, M., Kubiak, A., Młynarczyk, K., and Jesionowski, T. Synthesis, characterization and aging tests of functional rigid polymeric biocomposites with kraft lignin. *International Journal of Biological Macromolecules*, 178:344-353, 2021.

[41] Gil-Castell, O., Badia, J. D., Kittikorn, T., Strömberg, E., Martínez-Felipe, A., Ek, M., Karlsson, S., and Ribes-Greus, A. Hydrothermal ageing of polylactide/sisal biocomposites. Studies of water absorption behaviour and physico-chemical performance. *Polymer Degradation and Stability*, 108:212-222, 2014.

[42] Ventura, H., Claramunt, J., Rodríguez-Pérez, M. A., and Ardanuy, M. Effects of hydrothermal aging on the water uptake and tensile properties of PHB/flax fabric biocomposites. *Polymer Degradation and Stability*, 142:129-138, 2017.

[43] Chen, D., Li, J., and Ren, J. Influence of fiber surface-treatment on interfacial property of poly (l-lactic acid)/ramie fabric biocomposites under UV-irradiation hydrothermal aging. *Materials Chemistry and Physics*, 126(3):524-531, 2011.

[44] Siakeng, R., Jawaid, M., Asim, M., and Siengchin, S. Accelerated weathering and soil burial effect on biodegradability, colour and texture of coir/pineapple leaf fibres/PLA biocomposites. *Polymers*, 12(2):458-473, 2020.

[45] EL-Zayat, M. M., Mohamed, R. M., and Raslan, H. A. Evaluation of surface treatment and gamma irradiation on the performance of palm fiber/natural rubber biocomposites. *Journal of Macromolecular Science, Part A*, 57(5):344-354, 2020.

[46] Dutta, S., Karak, N., Saikia, J. P., and Konwar, B. K. Biodegradation of epoxy and MF modified polyurethane films derived from a sustainable resource. *Journal of Polymers and the Environment*, 18:167-176, 2010.